AIP Conference Proceedings

Removing biases from rotating shadowband radiometers

Cite as: AIP Conference Proceedings **2126**, 190017 (2019); https://doi.org/10.1063/1.5117714
Published Online: 26 July 2019

Frank Vignola, Josh Peterson, Fotis Mavromatakis, Stefan Wilbert, Anne Forstinger, Mike Dooraghi, and Manajit Sengupta

Removing Biases from Rotating Shadowband Radiometers

Frank Vignola[1,a)], Josh Peterson[1,b)], Fotis Mavromatakis[2,c)], Stefan Wilbert[3,d)], Anne Forstinger[3,e)], Mike Dooraghi[4,f)], Manajit Sengupta[4,g)]

[1]*Author Affiliation University of Oregon, Material Science Institute, Eugene, Oregon, 97403, USA*
[2]*Technological Educational Institute of Crete, Dept. of Electrical Engineering, Crete, Greece*
[3]*German Aerospace Center (DLR), Institute of Solar Research, Ctra de Senes s/n km4, Tabernas, Spain*
[4]*National Renewable Energy Laboratory, 15013 Denver W Pkwy, Golden, CO 80401, USA*

[a)]Corresponding author: fev@uoregon.edu
[b)]jpeters4@uoregon.edu ,[c)]fotis@staff.teicrete.gr, [d)]Stefan.Wilbert@dlr.de
[e)]Anne.Forstinger@dlr.de, [f)]Mike.Dooraghi@nrel.gov, [g)]manajit.sengupta@nrel.gov

Abstract. Three types of biases are examined for a Rotating Shadowband Radiometer (RSR): temperature bias, spectral bias, and deviation from a Lambertian cosine response. A step by step method is presented to illustrate how to use this information to develop a model for adjustment algorithms for a RSR. Comparisons are made with a RSR adjusted using the model and measure direct normal, diffuse, and global irradiance.

INTRODUCTION

A rotation shadowband radiometer (RSR) sometimes called a rotating shadowband irradiometer, is used to measure the global horizontal irradiance (GHI), the diffuse horizontal irradiance (DHI), and calculate the direct normal irradiance (DNI). The instrument is relatively simple to use and is less expensive than installing a suite of high quality instruments mounted on automatic tracker. The weakness of this system is that the RSR usually uses a photodiode-based pyranometer that has systematic bias.

Algorithms have been developed to remove these biases [1- 12] with varying degrees of success. Previously [1] we have developed a set of algorithms to remove the biases based on the spectral characteristics of the pyranometer and the spectral distribution of incident DNI and DHI irradiance. As with the other models, the deviation from the Lambertian cosine response, called the Angle of Incidence (AOI) effect was included. This model used the calibration of the DNI and DHI components at 45° for normalization of the algorithms and included a model for the DHI component under all weather conditions. A comparison was done for one month of data and it was assumed that the temperature effects were independent of the spectral distribution of the incident radiation. A more recent study [13] found that while small, the spectral dependence of the temperature effect should be taken into consideration approach. It was found that the temperature dependence of the algorithm was important and fell into two branches. A thorough study of RSR instruments compared to high quality GHI, DNI, and DHI measurements [14] showed that systematic biases still existed after the algorithms used to remove the biases were applied.

In many regions of the world, RSR are used to obtain the DNI component for analysis concentrating solar power (CSP) system performance. To accurately estimate the performance of CSP system, it is important that as many biases in the RSR measurements be removed as possible. What is new in this study is that the spectral dependence of the temperature effect is included in the analysis. Three factors are analyzed. First the spectral temperature effect is evaluated. Next the effect of the change in spectral distribution over the day is displayed. The angle of incident effects are the examined. The diffuse spectral effects for DHI for various sky conditions is then modeled. Comparisons of

SolarPACES 2018
AIP Conf. Proc. 2126, 190017-1–190017-10; https://doi.org/10.1063/1.5117714
Published by AIP Publishing. 978-0-7354-1866-0/$30.00

adjusted RSR measured irradiance and then compare to reference measurements. The steps used in the analysis for this paper are summarized in Appendix 1 and the formulas used in this analysis are given Table A2.1 in Appendix 2.

EXPERIMENTAL SETUP AND DATA

Data for the study comes from the University of Oregon Solar Radiation Monitoring Laboratory (UO SRML) in Eugene, Oregon. Rotating Shadowband Pyranometers (RSP) were run alongside high quality DNI measurements made with a Kipp & Zonen CHP 1 pyrheliometer, a Kipp & Zonen CMP22 pyranometer for GHI measurements, and a Schenk Star pyranometer for the DHI measurements. The RSP is an early version of the Irradiance RSR instrument that did not adjust the GHI, DHI, and DNI data. All instruments were also calibrated using an Eppley AHF cavity radiometer that has its calibration traceable to the WRR standard.

The CMP22 was calibrated using a shade/unshade methodology [17]. The Schenk Star pyranometer, mounted on an automatic tracker, was calibrated using the summation methodology [17]. Calibration data was analyzed in 10 second averages and the RSP was calibrated against one-minute data as the RSP generates data once a minute. For data used in other comparison, the DNI was from the CHP1 pyrheliometer and the DHI was from the Schenk Star. The data logger sampled the values every two seconds and output one-minute averages. The instruments were cleaned five days per week. The data set contains measurements from several similar instruments and data that significantly deviated from the other instruments were not used in this study. Such instances usually related to cleaning of the instruments or insects on the sensor. Periods of snow or ice on the instruments were also eliminated as well as rotation problems that occurred early in the morning. Data gathered when horizon obstructions affected the measurements were also eliminated. Data used in this study can be found at http://solardat.uoregon.edu.

Determining the Spectral Dependence of Temperature

Photodiodes behave similarly to solar cells that are measured at the short circuit current. Unlike photovoltaic modules (PV) when used to generate electricity, photodiodes increase their current output as temperature increases [16]. This mainly results from the kinetic energy boost given to electron hole pairs that were created with by photons with energy near the band gap energy. Electron hole pairs that were created by photons with much higher energy can more easily cross the band gap and are not significantly affected by the higher temperature. To see this affect, the relative responsivity of a reference cell was examined at temperatures at 25ºC, 35°C and 45°C. The data were taken at NREL using a standard lamp and RCO reference cells. The result of this experiment is shown in Fig. 1.

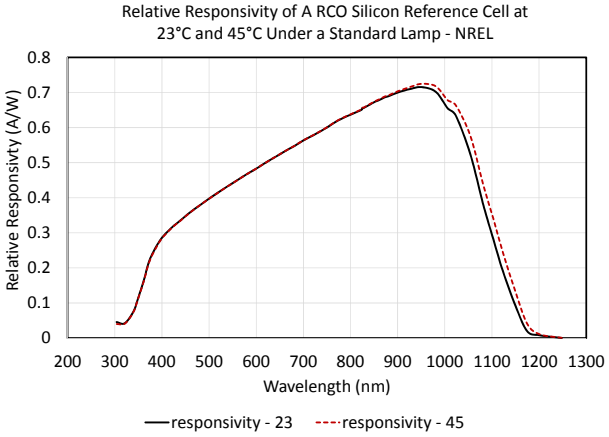

FIGURE 1. Relative responsivity of a RCO reference solar cell at 23°C and 45°C. Obtain from normalized percent quantum efficiency measurements made under a standard lamp at NREL.

The RCO reference cell measures the short circuit current on a silicon solar cell encased in glass similar to a PV module. The reference cell behaves much like a photodiode as both the reference cell and the photodiode measure

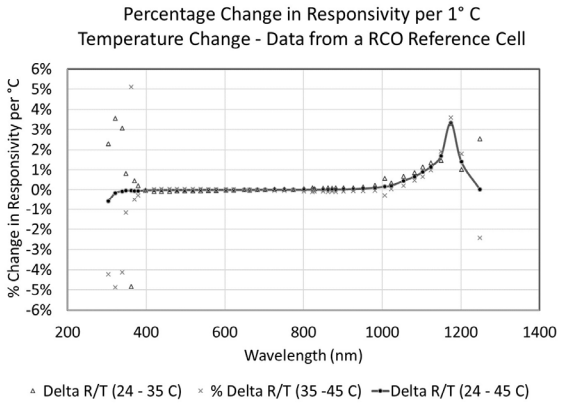

FIGURE 2. Illustration of the temperature spectral dependence using a silicon based RCO reference cell. There is little temperature dependence until the energy of the wavelength approaches that of the silicon band gap.

short circuit current of a silicon cell. The estimate of the silicon solar cell's temperature spectral dependence comes from quantum efficiency tests of a RCO reference cell at the National Renewable Energy Laboratory (NREL) conducted at temperature from 23°C to 45°C. The temperature's spectral behavior was obtained by comparing output for selected wavelengths at different temperatures. The spectral temperature dependence is illustrated in Fig. 2. Temperature increases reduces the required energy of the photon that is needed for an electron to jump the band gap, because of the electron's increased thermal energy.

The average of the temperature effect is similar to that found in other studies. The difference is that when the spectral distribution is shifted to longer wavelengths, such as during morning and evening hours, the temperature effect is enhanced. Over a day this is only about 0.5% difference, but over the year this is about a 2% to 3% effect.

To use the dependence of the temperature effect on the output of the pyranometer, a spectral model for the GHI and DHI irradiance over the day has to be determined. Reference spectra can be generated using spectral models such as SMARTS2 [18]. The incident spectral distribution is dependent on the constituents of the atmosphere and the amount of atmosphere through which the light travels, described as air mass. Aerosols, dust, and other atmospheric constituents absorb, scatter, and reflect the light as it travels through the atmosphere. This is referred to as Aerosol Optical Depth (AOD). Spectral models such as SMARTS2 generate spectral values using information such as AOD and air mass. The spectrum used in this study was one that were used in an earlier study [2] that was appropriate for the atmospheric conditions in Eugene, Oregon. The formulas obtained by modeling the effects of this spectrum on the temperature dependence will be different for locations with different spectral characteristics. On clear days, the temperature effect on diffuse irradiance is about twice as much as for the global irradiance because the diffuse spectrum is more peaked at the shorter wavelengths than the global spectrum. This is not necessarily true for partially cloudy and totally overcast days where the global and diffuse spectra to each other or identical. To better model the effect of the spectral characteristic of temperature on the instrument, GHI and DNI spectral measurements are necessary under all states of cloudiness. The slope of the broadband temperature correction obtained by [4] was T_{alpha} = 0.00082 1/K and the slope obtained by [7] was T_{alpha} = 0.0007 1/K. One can derive a broadband temperature correction by calculating the average responsivity at different temperatures using GHI spectra for ASTM G173 atmospheric conditions [15] and the relative responsivities shown in Fig. 1 at different temperatures. These responsivities can also be modeled using the spectral responsivity published by LI-COR [1] and the temperature dependent wavelength shift of the quantum efficiency for c-Si photovoltaic devices described by [16]. Using ASTM G173 atmospheric conditions [15] one can calculate the broadband temperature correction with the corresponding GHI spectrum for a given air mass and the temperature corrected spectral responsivities. This way, one obtains an T_{alpha} = 0.000834 1/K for an air mass of 4 and an T_{alpha} = 0.000786 1/K for an air mass of 1. This shows the effect of different spectra on the broadband temperature correction model. The formulas used to normalize all measurements to 25°C in this study can be found in Table A2.1 in Appendix 2.

The temperate measure in the NREL study was the temperature of the reference cell. To obtain the temperature of the RSP in this study, a model was derived relating the temperature of the pyranometer to the ambient temperature. This model was obtained from an RSR instrument in another location where both the ambient temperature and the sensor temperature was measured. This relationship is supplied in Table A2.1.

The next step in this process are to normalize all the GHI and DNI measurements to 25°C by dividing the original GHI(O) and DHI(O) with the respective temperature adjustment factor GHI(TA) and DHI(TA) (see Table 2A.1). The temperature adjusted data are labeled GHI(T), DHI(T), and DNI(T). DNI(T) was obtained by using eqn. 1.

$$DNI(T) = (GHI(T) - DHI(T))/\cos(SZA) \quad (1)$$

where SZA is the solar zenith angle.

The temperature adjusted values were then used to determine the responsivity over the day and the average responsivity for DHI(C) and DNI(C) were determined by averaging the responsivities determined between 44° and 46° degrees. The DNI(T) and DHI(T) values were then divided by the new responsivities at 45° and calibrated DNI(A) and DHI(A) values were obtained.

The Effect of Changing Spectral Distribution over the Day

The procedure to estimate the change in spectral distribution over the day is discussed in [2]. The DNI and DHI spectral values are multiplied by the corresponding spectral responsivity of the pyranometer and the average responsivity of the pyranometer is determined at various times of day. The changing responsivity over the day is then modeled as a function of SZA and the DNI(S) and DHI(S) spectral dependence functions are determined. These spectral functions are normalized to one at a SZA of 45°. The parameters obtained from this spectral modeling are in Table 2A.1. It is assumed that the DNI(S) spectral distribution does not change even when the sun is partially obscured by clouds. The spectrally normalized DNI(B) values are then obtained by dividing DNI(A) by DNI(S).

The diffuse spectrum does change significantly depending on cloudiness and the clear sky DHI is discussed in this section and the spectral effect under partially and totally cloudy skies will be treated in a later section. Like the DNI(B), the spectrally normalized clear sky DHI(B) is obtained by dividing DHI(A) by DHI(S).

The Effects of the Angle of Incident

Assume that the DNI(B) and the clear sky DHI(B) account for all the bias factors except the angle of incident (AOI) effects, the DNI(AOI) is obtained by dividing DNI(B) by the reference DNI(R). DNI(AOI) is then modeled as a function of SZA and the parameters are listed in Table 2A.1. By dividing DNI(B) by the modeled DNI(AOI), the final adjustment to the RSR's direct normal irradiance DNI(F) is obtained.

To separate the clear sky DHI from the cloudy sky DHI values, a plot of DHI(T) divided by DHI(R) is created (see Fig. 3). By looking at the plot of DNI(F) verses DHI(T) and manually marking clear sky periods, a formula was derived to identifying clear sky periods (2). The separation of clear and cloudy periods is illustrated in Fig. 3.

$$\text{If } DNI(F) > 14.285*DNI(T) - 285 \text{ then clear sky else cloudy} \quad (2)$$

For clear sky diffuse irradiance, the diffuse irradiance comes from over the whole sky dome and there is very little evidence of an AOI effect. This is not true during the early morning or late evening hours where circumsolar and horizon diffuse component constitute a majority of the diffuse irradiance. Therefore, the AOI is mostly one except for periods when the SZA is greater than 76°. The clear sky DHI(AOI, CS) is determined by dividing DHI(B) by the reference DHI(R) values. As with the DNI(F) component the final clear sky DHI(F,CS) value is determined by dividing DHI(B) by DHI(AOI, CS).

The data for the clear sky DHI(F, CS) forms a tight band that can be modeled while the cloudy sky DHI has a broad range of possible values. It is postulated that when the sky is totally overcast, the DHI(S) spectral distribution

will be very much like the DNI(S) spectral distribution. Under cloudless skies the clear sky diffuse adjustment is applicable. When it is partially cloudy, the DHI(S) is a combination of both (3).

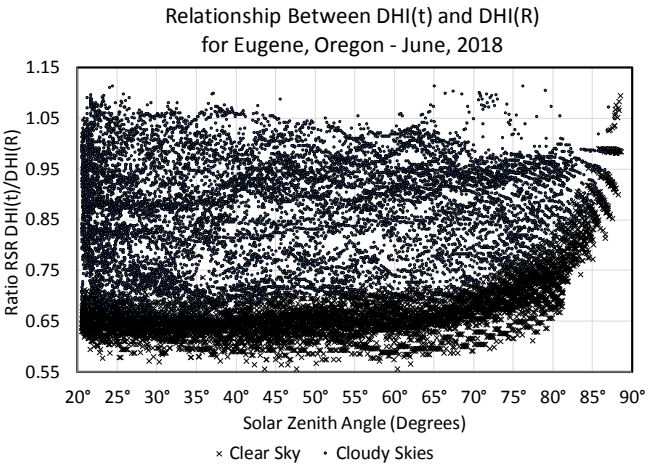

FIGURE 3. Ratio of all one-minute RSR DHI(t) divided by DHI(R) for June 2018 for Eugene, Oregon.

$$DHI(T)/DHI(R) = F(DHI(T)) * DHI(CS, Adjust) + (1 – F(DHI(T))) * DNI(S) \quad (3)$$

where DHI(CS, Adjust) is change made to the DHI(T) value under clear sky conditions. DHI(CS, Adjust) is equal to DHI(F,CS)/DHI(T). The data used to model F(DHI(T)) is generated using equation (4). The parameters obtained for F(DHI(T) in Eugene are given in Table A2.1.

$$F(DHI(T)) = [DHI(T)/DHI(R) – DNI(S)]/[DHI(CS, Adjust) – DNI(S)] \quad (4)$$

A function depending on DHI(T), F(DHI(T)), is created by modeling the data generated by Eq. 4. When this modeled function is used in Eq. 3, The cloudy day adjustment DHI(Cloudy, Adjust), the is modeled version of DHI(T)/DHI(R), is calculated using Eq. 3 with the modeled F(DHI(T)). DHI(F, Cloudy) is then DHI(T)/DHI(Cloudy, Adjust). The cloudy DHI(F, Cloudy) is then combined with the clear sky DHI(F,CS) and the adjusted direct normal and diffuse values are obtain. The adjusted GHI(F) values are obtained by the summation process of GHI(F) = DNI(F)*cos(SZA) + DHI(F).

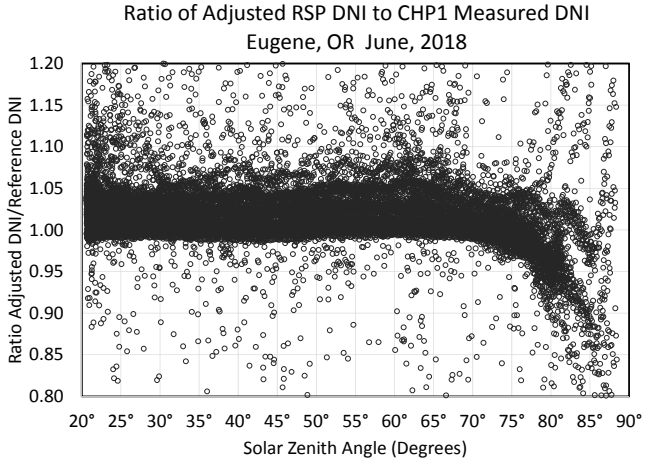

FIGURE 4. Comparison of RSP adjusted DNI(F) divided by the DNI(R) reference data from a CHP1 pyrheliometer for the month of June for all weather conditions.

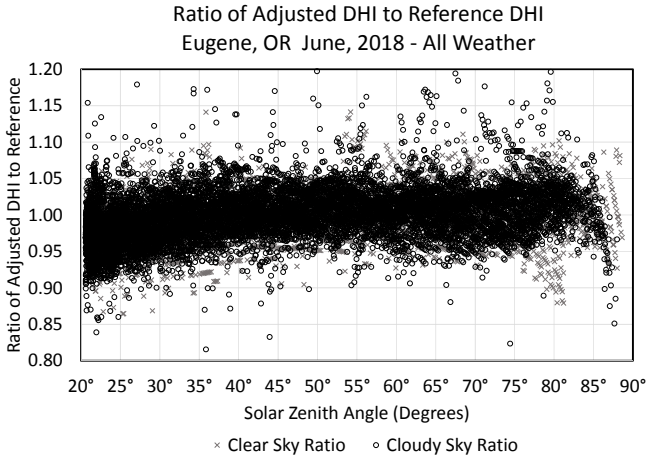

FIGURE 5. Comparison of RSP adjusted DHI(F) divided by reference DHI(R) from a Schenk Star pyranometer. Clear sky values are shown with "x's" and cloudy sky values with "o's".

RESULTS

The procedures for adjusting the DNI, DHI, and GHI parameters have been detailed above. The data from Eugene, Oregon in June of 2018 was used to develop and test the parameters. The match between the adjusted RSP data and the reference instruments are shown in Figs.res 4-6. The adjusted data agrees well with the measured reference data. This is somewhat to be expected because the data from June was used to help derive the adjustments. The DNI values show the greatest variations with zenith **angle, especially with zenith angles >75º. At these high** SZA values or equivalently large values of air mass changes in the spectral distributions have the largest effects and angle of incidence effects are the greatest. However, for most cases, the difference between the adjusted RSP values and the reference instruments is within 5%. These comparisons are made under all weather conditions where the differences between the one-minute sampling and the integrated averaging are likely to be large under partially cloudy weather conditions where DNI can changing rapidly. Under clear sky conditions, the fits to the data are better and don't have such large extremes.

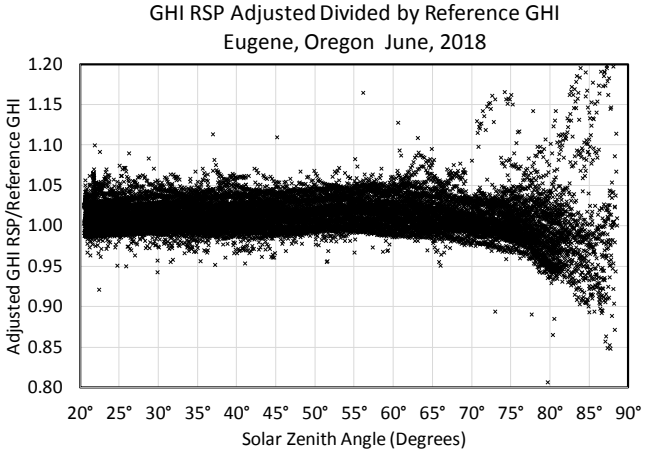

FIGURE 6. Ratio of adjusted RSP GHI and reference GHI obtained via the summation technique. It is only a large zenith angles (>75º) where difference start to appear.

CONCLUSIONS

By including the spectral characteristic of the temperature affect, the change in spectral effect on the performance of a RSR can be more accurately determined. The algorithms for adjusting the RSP are then modified accordingly and the new algorithms are tested against high quality DNI and DHI data in June. The step by step procedure is given in Appendix 1 and the parameters determined for the testing are given in Table A2.1. More testing is needed, especially during different times of year and at different locations.

There are several areas where improved data may be helpful. The temperature dependence was determined from a reference cell and not the pyranometer used in the experiments. Spectral temperature effects could be determined with more confidence if the spectral characteristics were determined for the specific pyranometer in use. Confidence in the results would also increase if the spectral dependence for the pyranometer came the pyranometer in use and not a "similar" one. The results might change if the spectral sensitivity of the instrument used in the study was measured.

More importantly, DNI and DHI spectral measurements obtained during the testing period would reduce the uncertainty associated with using a model to simulate the spectral distribution and estimate the effects.

Different parameterizations also should be studied. For example, the F(DHI(T)) used to study the spectral effects during partially cloudy periods could use a variable other than DHI(T), for example the ratio of DHI(T) to DNI(F). Other parameters such as the SZA could be changed to air mass.

ACKNOWLEDGEMENTS

The Bonneville Power Administration, the National Renewable Energy Laboratory, and the Energy Trust of Oregon are acknowledged for their support of the UO Solar Radiation Monitoring Laboratory. Without this support, this work would not be possible. This work was authored by Alliance for Sustainable Energy, LLC, the manager and operator of the National Renewable Energy Laboratory for the U.S. Department of Energy (DOE) under Contract No. DE-AC36-08GO28308. Funding provided by the U.S. Department of Energy Office of Energy Efficiency and Renewable Energy Solar Energy Technologies Office. The views expressed in the article do not necessarily represent the views of the DOE or the U.S. Government. The U.S. Government retains and the publisher, by accepting the article for publication, acknowledges that the U.S. Government retains a nonexclusive, paid-up, irrevocable, worldwide license to publish or reproduce the published form of this work, or allow others to do so, for U.S. Government purposes.

Abbreviation	Definition	Abbreviation	Definition
GHI(O)	Global horizontal irradiance - unadjusted	DHI(A)	Diffuse – calibration number applied
DHI(O)	Diffuse horizontal irradiance - unadjusted	DNI(S)	Direct Normal spectral adjustment factor
DNI(O)	Direct normal irradiance - unadjusted	DHI(S)	Diffuse clear sky spectral adjustment factor
T_{sensor}	Temperature of pyranometer	DNI(B)	Direct normal with spectral bias removed
GHI(TA)	Global temperature adjustment	DHI(B)	Diffuse with clear sky spectral bias removed
DHI(TA)	Diffuse temperature adjustment	DNI(AOI)	Direct normal angle of incidence factor
GHI(T)	Global data normalized to 25°C	DNI(F)	RSR Direct normal fully adjusted
DHI(T)	Diffuse data normalized to 25°C	DHI(AOI)	Diffuse clear sky angle of incidence factor
GHI(T)	Direct normal data normalized to 25°C	DHI(F, CS)	RSR Clear Sky Diffuse fully adjusted
GHI(R)	Reference global measurement	DHI(CS, Adjust)	Diffuse clear sky combined adjustment factors
DHI(R)	Reference diffuse measurement	DHI(Cloudy Adjust)	Diffuse cloudy sky spectral factor
DNI(R)	Reference direct normal measurement	DHI(F, Cloudy)	Diffuse cloudy sky fully adjusted
DNI(C)	Direct normal calibration number	DHI(F)	RSR diffuse fully adjusted
DHI(C)	Diffuse calibration number	GHI(F)	RSR global fully adjusted
DNI(A)	Direct normal – calibration number applied		
DHI(A)	Diffuse – calibration number applied		

APPENDIX 1 – PROCEDURES TO CALIBRATE AND ADJUST RSR VALUES

Steps involved to calibrate and adjust the RSR. The formulas and parameters used are given in Appendix 2.

1. Measure GHI(O), DHI(O), and DNI(O) from a RSR and over a clear day. Use the original data values and do not adjust these data values.
2. Obtain sensor temperature of the RSR over the same time-period
    a. If the instrument measures the sensor temperature obtain the sensor temperature measurements
    b. Otherwise develop, a model that translates ambient temperature ($T_{ambient}$) to sensor temperature (T_{sensor})
3. Determine how the average spectral responsivity of the RSR changes over the day. Correlate this change in responsivity with the air mass or solar zenith angle.
    a. If spectral data are not available, generate spectral values from a clear sky spectral model such as SMARTS2. Do this for the GHI, DHI, and DNI distributions [1, 2]. The spectral data should reflect the atmospheric conditions at the location where the instrument is used.
4. Determine the spectral responsivity of the RSR pyranometer at 25°C. Do this at several temperatures and determine how the spectral responsivity of pyranometer changes with temperature.
5. With the clear sky GHI and DHI spectral model, estimate temperature effects on the GHI and DHI measurements.
6. Normalize the GHI and DHI measurements to 25°C using the temperature measurements and GHI(O) and DHI(O) measurements. This process produces normalized temperature GHI(T) and DHI(T) values.
7. Calculate the temperature adjusted DNI(T) using the formula DNI(T) = (GHI(T) – DHI(T))/cos(SZA).
8. Determine the ratio of the DNI(T) obtained in step 8, to the reference DNI(R) value.
9. Average the ratio in Step 8 for SZA values between 44° and 46°. This value, DNI(C), is the change in calibration.
10. Use the calibration adjustment values DNI(C) to adjust the DNI(T). DNI(A) = DNI(T)/DNI(C).
11. Using the change in the DNI spectral distribution over the day and the spectral responsivity of the pyranometer at 25°C obtained in step 3, calculate the change in the DNI(S) spectral responsivity over the day. Normalize this value to one at the SZA of 45° [2].
12. Account for the effect of changing spectral distributions on DNI(A) by dividing by the modeled spectral effect function DNI(S). These new values are DNI(B).
13. Repeat Steps 8 through 12 using the DHI data and obtain, DHI(C), DHI(A), DHI(S) and DHI(B).
14. Estimate the angle of incident effects on the DNI by modeling the ratio of DNI(B) to the reference DNI(R).
    a. When DNI < 10 W/m^2 the data were not used because of the large uncertainty in these values.
15. Divide DNI(B) by DNI(AOI), the modeled fit to step 14. This yields DNI(F), the fully adjusted DNI value.
16. Steps to obtain the fully adjusted DHI(F) values
    a. Divide DHI(T) by the reference DHI(R) values
    b. Separate the data into clear sky and partially or totally cloudy skies. This can be done by comparing the DNI to the DHI values (see Eqn. 2).
    c. For the clear sky data, calculate the ratio of the adjusted DHI(B) value to the reference DHI(R) values. For large SZA values (>76°), determine the angle of incident affects, DHI(AOI,CS). Divide DHI(B) by this ratio to get the clear sky DHI(F) value.
    d. For totally cloudy periods, assume that the spectral distribution is similar to the DNI(S) and for partially cloudy periods the spectral distribution is a linear combination of DNI(S) spectral adjustment and the total DHI(CS, Adjust) adjustment. See Eqs. 3 and 4.
    e. Generate F(DHI(T)) values using Eq. 4. Model F(DHI(T)) as a function of DHI(T) using this data.
    f. The cloudy and partially cloudy sky DHI(F) are obtained by dividing DHI(T) by the modeled ratio value, DHI(T)/DHI(R), obtained in step 17.d.i. using the modeled F(DHI(T)) function.
17. Calculate the fully adjusted GHI(F) values using the summation process: GHI(F) = DNI(F)*Cos(SZA) + DHI(F).

APPENDIX 2 – FORUMULAS USED IN THIS ANALYSIS

TABLE A2.1: Formulas and parameters used in this article and associated with steps in Appendix 1.

Parameters	Equation or modeled result
T_{sensor}	$T_{sensor} = 1.897901+0.985771*T_{ambient}+0.0095347*GHI(O)-0.0000052293*GHI(O)^2$
GHI(TA)	$GHI(TA) = 1+(1-(\ 1.0016164789-0.0000024181*SZA+0.0000000301*SZA^2)) * (25-T_{sensor})$
DHI(TA)	$DHI(TA) = 1+(\ 1-(\ 1.00266706263-0.00022727465*SZA+0.0000074479*SZA^2$ $-0.00000010485*SZA^3 +0.00000000054*SZA^4\ )) * (25-T_{sensor})$
DNI(C)	DNI(C) = DNI(T)/DNI(R) averaged ratio to reference between SZA 44º-46º = 1.02345
DHI(C)	DHI(C) = DHI(T)/DHI(R) averaged ratio to reference between SZA 44º-46º = 0.633507
DNI(S)	$DNI(S) = 0.9962758-0.0007725*SZA +0.0000183*SZA^2$
DHI(S)	$DHI(S) = 1.30730596 - 0.0135366*SZA+0.00014936*SZA^2$
DNI(AOI)	DNI(AOI) = DNI(B)/DNI(R) - Generate data to be modeled as a function of SZA
DNI(AOI)	For SZA < 76º DNI(AOI) = $1.11077417 - 0.01282373*SZA + 0.00053605*SZA^2$ $- 0.000009377*SZA^3 + 0.000000057*SZA^4$ For SZA >= 76º DNI(AOI) = $489.72232030 - 18.57198910SZA + 0.23492048SZA^2$ $-0.00098896SZA^3$
DHI(AOI)	=DHI(B)/DHI(R) - Generate data to be modeled as a function of SZA
DHI(AOI)	For SZA > 76° DHI(AOI) = $-25.03643534 + 1.101530338*SZA - 0.01544087*SZA^2$ $+ 0.00007180*SZA^3$ For SZA <=76° DHI(AOI) = 1
DHI(F,CS)	DHI(B)/DHI(AOI)
DHI(CS,Adjuts)	DHI(S)*DHI(C)*DHI(AOI)
F(DHI(T))	For DHI(T) <5 W/m^2 F(DHI(T)) = 0 For 5< DHI(T) <70 W/m^2 $F(DHI(T)) = - 9.11718842 + 5.75219615*10^{-1}*DHI(T)$ $-1.49274615E-02*DHI(T)^2 + 1.75144373*10^{-4}*DHI(T)^3 -7.72331819*10^{-07}*DHI(T)^4$ DHI(T)>70 $F(DHI(T)) =-8.337568643*10^{-1} +7.21224815*10^{-3}*DHI(T) -2.799107376*10^{-5}*DHI(T)^2$ $+5.732372787*10^{-8}*DHI(T)^3 -5.660777562*10^{-11}*DHI(T)^4 +2.082958391*10^{-14}*DHI(T)^5$
DHI(Cloudy, Adjust)	DHI(Cloudy, Adjust) = F(DHI(T))*DHI(CS adjustment)+(1-F(DHI(T)))*DNI(S)
DHI(F, Cloudy)	DHI(F, Cloudy) =DHI(T)/DHI(Cloudy Adjust)

REFERENCES

1. Frank Vignola, Josh Peterson, Stefan Wilbert, Philippe Blanc, Norbert Geuder, and Chris Kern New methodology for adjusting rotating shadowband irradiometer measurements Citation: AIP Conference Proceedings 1850, 140021 (2017)
2. Vignola, F., Z. Derocher, J. Peterson, L. Vuilleumier, C. Félix, J. Gröbner, N. Kouremeti, 2016: Effects of changing spectral radiation distribution on the performance of photodiode pyranometers. – *Solar Energy* 129, 224–235.
3. Michalsky, J.J., R. Perez, L. Harrison, B.A. LeBaron, 1991. Spectral and temperature correction of silicon photovoltaic solar radiation detectors. – Solar Energy 47, 299–305
4. King, D., Myers, D., 1997. Silicon-photodiode pyranometers: operational characteristics, historical experiences, and new calibration procedures. In: 26th IEEE Photovoltaic Specialists Conference, September 29–October 3, 1997, Anaheim, California
5. Vignola, F., 1999: Solar Cell Based Pyranometers: Evaluation of the Diffuse Response. – Proc. 1999 American Solar Energy Society Conference, 255–260, American Solar Energy Society, Boulder, Colorado, USA.
6. Vignola, F., 2006: Removing Systematic Errors from Rotating Shadowband Pyranometer Data. – Proc. 2006 American Solar Energy Society Conference, American Solar Energy Society, Boulder, Colorado, USA.
7. Geuder, N., Pulvermüller, B., et al., 2008. Corrections for rotating shadowband pyranometers for solar resource assessment. Soc. PhotoOpt. Instrum. Eng.
8. Geuder, N., R. Affolter, O. Goebel, B. Dahleh, M. Al Khawaja, S. Wilbert, B. Pape, B. Pulvermueller, 2010: Validation of direct beam irradiance measurements from rotating shadowband pyranometers in a different climate. – 16th SolarPACES Conference, 21–24. September 2010, Perpignan, France.
9. Geuder, N., R. Affolter, B. Kraasb, S. Wilbert, Long-term Behavior, Accuracy and Drift of LI-200 Pyranometers as Radiation Sensors in Rotating Shadowband Irradiometers (RSI). *Energy Procedia* 49: 2330-2339, 2014.

10. Stefan Wilbert, Stefan Kleindiek, Bijan Nouri, Norbert Geuder, Aron Habte, Marko Schwandt, Frank Vignola, Uncertainty of Rotating Shadowband Irradiometers and Si-Pyranometers Including the Spectral Irradiance Error. AIP Conference Proceedings 1734, 150009 (2016); https://doi.org/10.1063/1.4949241
11. Augustyn, J., T. Geer, T. Stoffel, E. Kern, R. Little, F. Vignola, R. Kessler, 2002: Improving the accuracy of low cost measurement of direct normal solar irradiance. – Proc. 2002 American Solar Energy Society Conference, 329–334, American Solar Energy Society, Boulder, Colorado, USA.
12. Augustyn, J., T. Geer, T. Stoffel, F. Vignola, R. Kessler, E. Kern, R. Little, B. Boyson, 2004: Update of algorithm to correct direct normal irradiance measurements made with a rotating shadow band pyranometer. – Proc. 2004 American Solar Energy Society Conference, 295–302. American Solar Energy Society, Boulder, Colorado, USA
13. Vignola, F., Josh Peterson, Rich Kessler, Mike Dooraghi, and Manajit Sengupta, Fotis Mavromatakis, 2018. Evaluation of Photodiode-based Pyranometers and Reference Solar Cells on a Two-Axis Tracking System. *IEEE PVSC Conference*, Hawaii, 2018.
14. Laurent Vuilleumier, Christian Félix, Frank Vignola, Philippe Blanc, Jordi Badosa, Andreas Kazantzidis and Bertrand Calpini Performance Evaluation of Radiation Sensors for the Solar Energy Sector, Meteorologische Zeitschrift, PrePub DOI 10.1127/metz/2017/0836
15. [ASTM, 2012] ASTM. 2012. G 173_03. In Standard Tables for Reference Solar Spectral Irradiances: Direct Normal and Hemispherical on 37° Tilted Surface. ASTM International: ASTM.
16. Hishikawa, Yoshihiro, Masahiro Yoshita, Hironori Ohshima, Kengo Yamagoe, Haruya Shimura, Ayumi Sasaki, and Takashi Ueda, 2018. Temperature dependence of the short circuit current and spectral responsivity of various kinds of crystalline silicon photovoltaic devices, Japanese Journal of Applied Physics 57, 08RG17 (2018)
17. Vignola, F., Joseph Michalsky, Tom Stoffel, 2012. Solar and Infrared Radiation Measurements, Taylor & Frances Group, Boca Raton, Florida.
18. https://rredc.nrel.gov/solar/models/smarts/relatedrefs/smarts295_users_manual_pc.pdf.